Theor Chim Acta (1994) 89: 157–168

Theoretica Chimica Acta

MCSCF reaction-path energetics and thermal rate-constants for the reaction of ^3NH with H_2

Josef Ischtwan[1,*], Peter Schwerdtfeger[1], Sigrid D. Peyerimhoff[2], Michael A. Collins[3], Trygve Helgaker[4], Poul Jørgensen[5], Hans Jørgen Aa. Jensen[6]

[1] Department of Chemistry, University of Auckland, Private Bag 92019, Auckland, New Zealand

[2] Institut für Physikalische und Theoretische Chemie, Universität Bonn, Wegelerstrasse 12, D-53115 Bonn, Germany

[3] Research School of Chemistry, Australian National University, GPO Box 4, Canberra, ACT 2601, Australia

[4] Department of Chemistry, University of Oslo, Blindern, N-Oslo 3, Norway

[5] Department of Chemistry, Aarhus University, DK-8000 Aarhus C, Denmark

[6] Department of Chemistry, Odense University, DK-5230 Odense M, Denmark

Received February 8, 1994 / Accepted April 27, 1994

Summary. The intrinsic reaction-path, reactants, transition state and products for the reaction of NH ($^3\Sigma^-$) + H_2 ($^1\Sigma_g^+$) → NH_2 ($^2B_1$) + H (^2S) involving the lowest triplet electronic state of NH_3 were calculated using multi-configuration (MC) SCF methods. The calculated change of internal energy for the reaction of 11.0 kcal mol^{-1} agrees with the experimental value within 2 kcal mol^{-1}. The barrier to reaction is 23.4 kcal mol^{-1} high. The harmonic MCSCF reaction-path potential was calculated and canonical variational transition state theory calculations of the rate constants performed over a temperature range from 400 to 2500 K. The computed rate constants are generally two orders of magnitude smaller than those of the comparable reaction of OH with H_2, whereas those of the reverse reaction are by a factor of 20 larger than those of OH_2 with H.

Key words: Multi-configuration self-consistent field method – Reaction-path energetics – Thermal rate-constants

1 Introduction

Theoretical approaches to the dynamics of unimolecular and bimolecular reactions in the gas phase [1,2] involving polyatomic molecules are based on Born–Oppenheimer potential energy hypersurfaces (PES). Such a PES should describe the molecular interaction-potential in regions of the configuration space which are accessible by the reacting or rearranging molecules. For reactions near threshold conditions it is often assumed that a reaction-path potential [1,2] describing the PES in the vicinity of a minimum energy path [3] (MEP) suffices.

* FEODOR-LYNEN Alexander von Humboldt Fellow
Correspondence to: P. S. (Auckland) or M. A. C. (Canberra)

This assumption is based on the chemical picture that only part or parts of the molecules participate in the reaction or rearrangement, whereas other parts remain spectators.

Considerable progress has been made in recent years in the computationally efficient and accurate determination of minimum energy reaction-paths for small polyatomic molecules using *ab initio* molecular orbital methods [4]. For a molecule consisting of N atoms ($N < 7$) [5], the molecular energy, energy gradients and force-constants, V, $\boldsymbol{G}$ and $\boldsymbol{F}$, can be routinely calculated by *ab initio* molecular orbital methods at a sequence of points on a MEP. The reaction-path potential can then be approximated by a second order Taylor-expansion (T denotes the transpose)

$$V(\xi;s) = V(\xi_0;s) + \boldsymbol{G}[\xi - \xi_0;s] + \tfrac{1}{2}[\xi - \xi_0;s]^{\mathrm{T}}\boldsymbol{F}[\xi - \xi_0;s] \qquad (1)$$

in $3N - 6$ internal coordinates ξ, around configurations on the MEP, parametrized by a value for the reaction coordinates, s. Such a potential describes – within the validity of the *ab initio* approximation employed – the PES accurately in the direction of the reaction-path. However, the accuracy of the potential in the transverse directions [1,2] to the path is limited by the magnitude of the anharmonicities [5]. A conventionally used coordinate system for determining a reaction-path is the massweighted Cartesian coordinates [1,2], and the corresponding path of steepest descents is referred as Fukui's intrinsic reaction path (IRP) [3].

Ab initio methods employed for determining the topology of a surface and the MEP for a reaction should be based on a continuous description of the electronic wave function for all molecular arrangements. Single reference Hartree–Fock (HF) and Møller–Plesset perturbation (MP) theory methods [14] are adequate for the partial description of chemical bonding effects in closed shell electronic ground states. However, even for these simple cases, most single-configuration reference methods fail to describe the breaking of bonds which result in open shell electronic states for the fragment molecules [6]. In contrast, multi configuration *ab initio* methods, like multi reference configuration interaction [7] and multi configuration self consistent field (MCSCF) [8] methods allow a quantitatively correct description of the electronic state in the sense that they continuously reflect the change in the nature of the electronic state for different nuclear arrangements. A considerable advance for the determination of hypersurfaces (such as Eq. (1)) for bimolecular reactions is provided by the development of efficient MCSCF molecular energy, gradient and Hessian programs [9, 10].

We report here the IRP for the reaction [11]

$$\mathrm{NH}\ (^3\Sigma^-) + \mathrm{H_2}\ (^1\Sigma_g^+) \rightarrow \mathrm{NH_2}\ (^2\mathrm{B_1}) + \mathrm{H}\ (^2\mathrm{S}) \qquad (2)$$

calculated with an MCSCF method. This reaction involves the lowest electronic state of $^3NH_3$. The harmonic potential, Eq. (1), is evaluated at a dense sequence of points on this path and thermal rate-constants are computed using canonical variational transition state theory (CVTST) [2].

Ground-state ^{3}NH tends to undergo addition toward radical species [12] and olefins [13] in the gas-phase, whereas H-abstraction from olefins is highly inefficient. Molecular hydrogen and ^{3}NH are chosen in this study as the simplest prototype of reactants and as practically important in relation to their possible participation in chemical cycles involved in the upper atmosphere.

Section 2 describes the *ab initio* methods used. Section 3 compares the *ab initio* calculated energetics of reaction (2) with the experimental data, and Sect. 4 describes the reaction-path rate-constants for reaction (2). Section 5 contains concluding remarks.

2 *Ab initio* method

A reaction-path for this reaction has been described previously in an *ab initio* study by Fueno et al. [11]. They used the multireference double-excitation configuration interaction (MR-DCI) [7] method with a split-valence 4-31G basis set [14] plus one set of polarization functions on each atom. The calculated reaction path describes repulsive molecular arrangements and leads over a saddle point in which all atoms lie in one plane (C_s symmetry). Their calculated change in internal energy, ΔE, for reactants and products overestimates the experimentally inferred value [11] by 6.5 kcal mol^{-1}.

An *ab initio* method used for calculating the surface (1) for reaction (2) must be a compromise between accuracy and computational expense. For achieving a qualitatively correct description of the bond-rupture and formation processes, the electronic wave function has to describe continuously the change of the electronic structure for the molecular arrangements during the reaction. The electronic structure changes taking place along the minimum energy-path of reaction (2) involve the eight valence electrons of triplet NH_3.

A standard way of choosing a configuration space has been to use a complete active space [8] (CAS) wave function and to include in the active space one correlating molecular orbital (MO) for each strongly occupied active orbital. However, a more quantitative measure for the inclusion of MOs in the correlation treatment are their natural orbital occupation numbers (NO). For some cases it has been shown that for the simplest choice of a CAS configuration space it is necessary to include two correlating orbitals for some of the strongly occupied active orbitals [15]. We have tested two choices of active spaces for the CAS wave function for the eight valence electrons of triplet NH_3, both of which asymptotically correlate with a 2-electrons-in-2 MOs CAS for molecular hydrogen. These CAS wave functions are constructed by distributing eight valence electrons in all possible ways among nine active orbitals (7 a', 2 a'' in C_s symmetry) (CAS9) resulting in 3780 configuration state functions (CSF), and among a larger active space of 9 a' and 2 a'' orbitals (CAS11) resulting in a CAS wave function with 25452 CSFs. In Tables 1–3, The NO are listed for CAS9 and CAS11 for the fragments and the $^3NH_3$ saddle point. These NO are compared with those of a spin-unrestricted single-reference second order Møller–Plesset (MP2) wave function correlating the eight valence electrons (all evaluated for the same geometries at the MP2 stationary points). A comparison with the MP2 values shows that the CAS11 approximation consistently includes the correlation of the radical electrons for the asymptotes in contrast to the CAS9 approximation. In the CAS9 wave function the radical electrons of ^3NH (Table 1) are uncorrelated giving rise to a discontinuous correlation treatment along the minimum energy path for reaction (2), as these radical electrons and MOs contribute to the NH bonds and correlation of NH_2 (Table 2). The CAS11 wave function describes continuously the correlation of those MOs and electrons for both asymptotes as well as for the transition complex $^3NH_3$ at the saddle point (Table 3).

Table 1. Natural orbital occupation numbers in NH ($^3\Sigma^-$)[a]

Active orbital numbers	Irreducible representations (C_{2v})											
	MP2				CAS11				CAS9			
	a_1	b_1	b_2	a_2	a_1	b_1	b_2	a_2	a_1	b_1	b_2	a_2
1	1.978	0.994	0.994	0.003	1.985	0.995	0.995	—	1.991	1.0	1.0	—
2	1.968	0.007	0.007	—	1.976	0.007	0.007	—	1.979	—	—	—
3	0.020	0.004	0.004	—	0.020	—	—	—	0.019	—	—	—
4	0.009	—	—	—	0.009	—	—	—	0.006	—	—	—
5	0.006	—	—	—	0.005	—	—	—	0.005	—	—	—
6	0.003	—	—	—	—	—	—	—	—	—	—	—

[a] Calculated at the MP2 optimised geometry

Table 2. Natural orbital occupation numbers in NH_2 ($^2B_1$)[a]

Active orbital numbers	Irreducible representations (C_{2v})											
	MP2				CAS11				CAS9			
	a_1	b_1	b_2	a_2	a_1	b_1	b_2	a_2	a_1	b_1	b_2	a_2
1	1.981	0.993	1.969	0.005	1.986	0.995	1.975	—	1.989	0.995	1.981	—
2	1.970	0.007	0.019	—	1.975	0.008	0.020	—	1.981	0.007	0.019	—
3	0.017	0.004	0.007	—	0.018	—	0.006	—	0.017	—	—	—
4	0.010	0.0006	0.0012	—	0.011	—	—	—	0.011	—	—	—
5	0.006	—	—	—	0.006	—	—	—		—	—	—
6	0.004	—	—	—	—	—	—	—	—	—	—	—
7	0.001	—	—	—	—	—	—	—	—	—	—	—

[a] Calculated at the MP2 optimised geometry

Table 3. Natural orbital occupation numbers in NH_3[a]

Active orbital numbers	Irreducible representations (C_s)					
	MP2		CAS11		CAS9	
	a'	a''	a'	a''	a'	a''
1	1.980	0.993	1.985	0.995	1.989	0.995
2	1.969	0.007	1.973	0.008	1.980	0.008
3	1.962	0.004	1.967	—	1.971	—
4	0.997	0.004	1.000	—	1.000	—
5	0.025	—	0.030	—	0.028	—
6	0.018	—	0.020	—	0.019	—
7	0.009	—	0.010	—	0.010	—
8	0.007	—	0.007	—	—	—
9	0.005	—	0.005	—	—	—

[a] Evaluated at the geometry of the MP2 saddle point

As a basis-set which satisfies the requirements for flexibility and computational affordability, we chose the Dunning 5*s*/4*p* contraction of the Huzingaga 10*s*/6*p* double-zeta basis for nitrogen and the 3*s* contraction for the 5*s* hydrogen primitive set [16]. They are augmented by one set of polarisation functions on each atom with exponents of 0.913 for nitrogen and 0.75 for hydrogen [14]. This results in 41 contracted basis functions. The electronic structure calculations have been performed using the GAUSSIAN90 program package [17] for the spin-unrestricted HF and MP2 methods and the SIRIUS/ABACUS program package [9, 10] for the CAS treatment. Structures were fully optimized at the CAS, HF and MP2 levels of theory for reactants, transition state and products of reaction (2). For the HF and MP2 calculations, spin-unrestricted wavefunctions for the open-shell systems have been used and in addition, the MP2 calculations included the nitrogen 1*s*-electrons in the correlation treatment. The spin-contamination for the HF and MP2 wave functions is less than 1% for all equilibrium structures of the fragments and less than 3% for the saddle point.

3 Structures, vibrational frequencies and energetics

The optimized geometries are shown in Table 4. The maximum difference between the calculated bond lengths and the experimental values for the fragments is 0.015 Å, with the MP2 and CAS predicted bond lengths being closer to the experimental values. Significant differences are found for the intermolecular NH bond lengths at the saddle point. At the HF level the intermolecular NH bond of the HN–H–H complex is 0.048 Å shorter than the CAS result, while the corresponding MP2 value lies between these two. The bond lengths between the nearest neighbour H atoms are 0.06 and 0.029 Å larger at the HF level compared to the MP2 and CAS bond lengths, respectively. Thus, in the HF approximation the

Table 4a. Geometry of the $^3NH_3$ saddlepoint[a]

	R (NH^1)	R (NH^2)	R (H^2H^3)	α (H^1NH^2)	β (NH^2H^3)
HF	1.017	1.194	1.005	100.3	170.0
MP2	1.032	1.211	0.945	98.8	168.0
CAS11	1.041	1.242	0.976	99.5	166.8

[a] Planar (C_s) geometry; bond lengths R in Ångstrøms and angles α, β in degrees. The labelling of the atoms is defined in Fig. 1.

Table 4b. Geometries of ^3NH, H_2 and $^2NH_2$

	^3NH	H_2	NH_2	
	R (NH)	R (HH)	R (NH)	α (HNH)
Hartree–Fock	1.023	0.727	1.011	104.7
MP2	1.034	0.730	1.024	102.9
CAS11	1.048 [1.038]	0.748 [0.742]	1.033 [1.024]	103.7 [103]

Notation as in Table 4; NH_2 has C_{2v} symmetry; experimental values from Ref. [19] are set in brackets

Table 5. Barrier heights, $\Delta E\#$, and changes in internal energy ΔE, for reaction (2)[a]

	Hartree–Fock	MP2	CAS11	Experiment
ΔE (ΔE_0)	20.8 (21.8)	11.3 (12.0)	10.0 (11.0)	(9.9)
$\Delta E\#$ ($\Delta E_0\#$)	35.2 (36.5)	22.6 (22.7)	23.2 (23.4)	

[a] Relative to the energy of NH + H_2 (in kcal mol^{-1}); values in parenthesis include ZPE; experimental value (extrapolated to 0 K) is taken from Ref. [11(b)]

saddle point lies late in the reaction-path of reaction (2), whereas the MP2 and CAS saddle points are shifted significantly more towards the reactant side. This is qualitatively consistent with Hammond's postulate [18]. The late saddle point of a more "NH_2–H structure" correlates with the calculated change of internal energy of 20.8 kcal mol^{-1} (Table 5) for HF, whereas the earlier MP2 and CAS saddle points give significantly lower values of 11.3 and 10.0 kcal mol^{-1}, respectively.

The accuracy of the *ab initio* methods employed may be judged using the experimental value for the change in internal energy for the reaction and the variation of the barrier height with improvement of the method. Table 5 lists the experimental (extrapolated to 0 K) change of internal energy, ΔE_0, together with our calculated results [including zero-point vibrational energy (ZPE) corrections]. The qualitatively correct behaviour of the CAS11-wave function in these dissociation limits is reflected in the good agreement of ΔE_0 with the experimental result (Table 5). In contrast, the HF value differs from the experimental value by about 10 kcal mol^{-1}, overestimating ΔE_0 by 100%. The HF barrier is about 12 kcal mol^{-1} larger than the similar MP2 and CAS barriers. Obviously, the CAS approximation includes a significant portion of the dynamical correlation.

Vibrational harmonic frequencies of the optimised structures are listed in Table 6 along with the experimentally observed (anharmonic) frequencies [19]. HF harmonic frequencies generally overestimate the experimentally observed frequencies by more than 10%. The CAS harmonic frequencies for H_2 and NH agree with the experimental values (of the anharmonic frequencies) within about 50 cm^{-1}, compared to an overestimation by 130–250 cm^{-1} by the MP2 approximation. For NH_2 the CAS and MP2 frequencies overestimate the experimental values by less than 10%.

The three approximations to the vibrational frequencies at the saddle point differ most for the imaginary frequency. The CAS-value of 1527 cm^{-1} for the NH_2 bending mode is adiabatically correlated with a lower value for a combined bending/H–H stretching mode of 1273 cm^{-1}. The HH-stretching frequency of 4355 cm^{-1} drops significantly to a value of 1487 cm^{-1} at the saddle point for a combined HH-stretch/anti-symmetric NH stretching mode. The NH stretching frequency remains virtually unchanged at the saddle point. The frequency of 668 cm^{-1} corresponds to an in-plane hindered internal rotation of the HN–H–H moieties indicating that an exchange process for

$$NH + H'H'' \rightarrow HN\text{–}H'\text{–}H'' \text{ (TS)} \rightarrow H'N\text{–}H\text{–}H'' \text{ (TS')} \rightarrow NH' + HH'' \qquad (3)$$

is energetically unfavourable near the abstraction saddle point (TS). However, this frequency approaches zero asymptotically for NH_2 + H making the exchange process more likely to occur. Moreover, we have verified by further calculations that there are out-of-plane exchange pathways of much lower energy than the

Table 6. Vibrational frequencies[a]

	$H_2 + {}^3NH$				NH_3 ($^3A''$)				NH_2			
	HF	MP2	CAS	Expt.	HF	MP2	CAS	Expt.	HF	MP2	CAS	Expt.
	4726.9	4658.6	4355.3	4405	3592.4	3446.7	3303.6	—	3705.5	3579.2	3342.2	3220
	3519.8	3411.6	3239.5	3282	1514.7	1652.4	1487.1	—	3612.9	3473.1	3441.9	3197
					1357.7	1316.1	1273.6	—	1628.5	1528.0	1527.5	1497
					941.0 (a'')	1009.5 (a'')	952.7 (a'')	—				
					674.4	657.2	668.2	—				
					2779.9(i)	2389.8(i)	2262.4(i)	—				
ZPE	0.0188	0.0184	0.0173	—	0.0184	0.0185	0.0175	—	0.0204	0.0195	0.0189	

[a] In cm^{-1}; experimental frequencies of the fragments are taken from Ref. [19]; the zero point vibrational energy (or their sum) is given in hartrees. The imaginary frequency corresponding to the reaction-path mode is indicated as (i)

in-plane pathways. The frequency of 952 cm^{-1} corresponds to an out-of-plane vibration. Zero-point vibrational energies, calculated from the harmonic frequencies, are also reported in Table 6.

4 Intrinisic reaction-path, transverse mode frequencies and CVTST rate constants

The CAS steepest descent path in massweighted Cartesian coordinates from the saddle point to reactants and products has been determined using the local-quadratic approximation algorithm [4], which uses the molecular gradients and Hessian calculated at each step for an optimal estimate of the step-length in the direction of the path. The step-length varies between 0.01 and 0.1 a.u., depending on the anharmonicity of the potential in the direction of the reaction-path. At a total of 75 points the complete set of energy, energy gradients and second derivatives of Eq. (1) were calculated. The interpolated energy-profile and the internuclear distances along this path as functions of the intrinsic reaction coordinate (IRC) [4] are shown in Figs. 1 and 2, respectively. This path describes the approach of H_2 to ^3NH in plane, starting from an intermolecular distance of about 6.5 bohr, to the planar saddle point HN–H–H. The abstraction of the directly connected H atom is followed up to a H–H separation of about 4.0 bohr. As

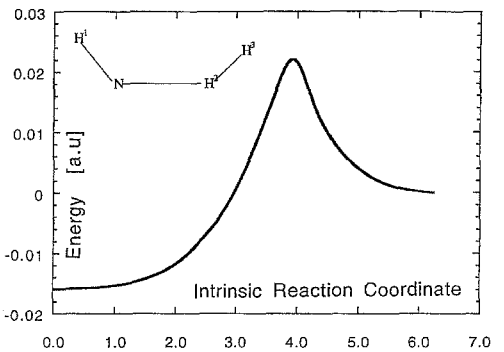

Fig. 1. Energy profile along the IRP for the reaction NH ($^3\Sigma^-$) + H_2 ($^1\Sigma_g^+$) → NH_2 ($^2B_1$) + H (^2S). The intrinsic reaction coordinate is given in atomic units. The geometry of the saddle point is given schematically indicating the labelling of the atoms

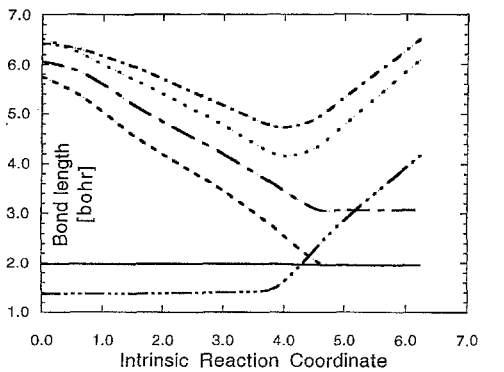

Fig. 2. Internuclear distances of $^3NH_3$ along the IRP as in Fig. 1. The solid horizontal curve represents the bond length R (N–H^1); the lowest curve represents R (H^2–H^3), the remaining curves are (in ascending order) R (N–H^2), R (H^1–H^2), R (H^2–H^3), R (H^1–H^3)

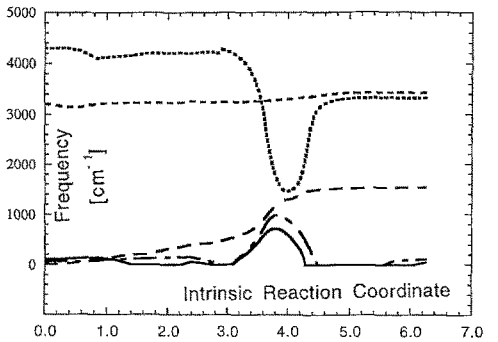

Fig. 3. Projected harmonic frequencies of the transverse modes along the IRP. The assignment of the modes is given in Table 3 and is described in the text

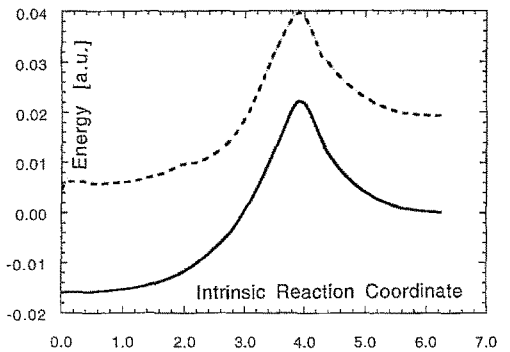

Fig. 4. Energy profile of the vibrationally adiabatic potential energy along the IRP. The IRP potential of Fig. 1 (solid line) is shown for comparison

mentioned before, the intramolecular NH-bond remains virtually unchanged on this path. The HH-bond begins to elongate shortly before the saddle point and the originally internuclear NH-bond reaches its value in the NH_2 molecule shortly after the saddle point.

In the reaction-path picture of chemical reactions, the vibrational frequencies and generalized normal modes [1,2] change continuously along a path from reactant to product. For nonstationary points along the IRP, the vibrational frequencies are determined by projecting the translational and rotational degrees of freedom and the reaction-path direction from the massweighted Cartesian force constant matrix [1,2]. Figure 3 shows the frequencies of the $3N-7$ transverse modes calculated in the harmonic approximation along the path of reaction (2). The frequency for the intramolecular NH stretch stays virtually unchanged on the path (at ca. 3200 cm^{-1} in Fig. 3), whereas the frequency for the HH bond adiabatically transforms to the frequency of the combined bending/HH stretch at the transition complex and to the frequency of the antisymmetric stretch/bending mode of NH_2 (starting at ca. 4300 cm^{-1} in Fig. 3). The bending frequency of NH_2 vanishes for the reactant.

If we assume that motion along the reaction coordinate is separable from motion in the remaining degrees of freedom [1,2], the most reasonable barrier shape for describing tunneling dynamics is the vibrationally adiabatic ground-state potential energy curve [20]. This is the sum of the potential energy of the reaction path and the zero-point vibrational energies for the transverse vibrations on the path. Figure 4 compares the vibrationally adiabatic ground-state potential with

Table 7. CVTST thermal rate constants for reaction (2), k_1, and the reverse reaction, k_2

Temperature	k_1	k_2
400	2.42 (− 24)	3.85 (− 18)
600	5.81 (− 20)	9.19 (− 16)
1000	2.39 (− 16)	9.64 (− 14)
1500	2.08 (− 14)	1.29 (− 12)
2000	1.91 (− 13)	4.46 (− 12)
2500	4.29 (− 13)	5.44 (− 12)

[a] Temperature in Kelvin and rate constants in $cm^3 molecule^{-1} s^{-1}$; powers of 10 are given in parenthesis.

the Born–Oppenheimer potential along the path. The geometries of the saddle points for the vibrational ground-state and the Born–Oppenheimer surfaces are identical.

The reaction rates for reaction (2) and for the reverse reaction have been calculated for a temperature range 400–2500 K using canonical variational transition-state theory (CVTST) [2]. The vibrational densities of states have been evaluated quantum mechanically in the harmonic approximation, and the rotation has been modelled as that of a classical rigid rotor. The degeneracies, d_{el}, of the electronic states in the electronic partition functions for the reactants NH, H_2 (and of H, NH_2 for the reverse reaction) and for the variational transition state complex are $d_{el}[NH\ (^3\Sigma^-)] = 3$, $d_{el}[H_2\ (^1\Sigma^+)] = 1$, $d_{el}[NH_3\ (^3A'')] = 3$, $d_{el}[NH_2\ (^2B_1)] = 2$, $d_{el}[H\ (^2S)] = 2$. The transition state is determined variationally by minimising the reaction rate as a function of the location of the transition state on the MEP. The electronic energy of the transition state is taken to be that of the corresponding point on the MEP. The global surface of $^3NH_3$ possesses six distinct symmetry-equivalent reaction-paths for reaction (2). The exchange symmetries of the $^3NH_3$ complex and of the reactants have been taken into account by the appropriate symmetry numbers, σ [21], in the rate constants ($\sigma(NH_3) = 1$, $\sigma(NH_2) = 2$, $\sigma(NH) = 1$, $\sigma(H_2) = 2$, $\sigma(H) = 1$). The CVTST results are listed in Table 7. For temperatures below 1500 K the variationally determined transition state is located at the saddle point of the vibrationally adiabatic ground-state surface. For temperatures above 1000 K the reaction rates for reaction (2) are generally two to three orders of magnitude smaller than those reported for the analogous reaction of OH with H_2 [22] which is exothermic. The surface for the latter reaction has a much smaller barrier of 6.2 kcal mol^{-1}. The occurrence of reaction (2) has not yet been confirmed experimentally. The rate-constants for the reverse reaction are a factor of 20 larger than those for the analogous reaction of OH_2 with H [23], for which a barrier of about 21 kcal mol^{-1} has been determined.

The available experimental studies on the reactions of triplet NH in the gas phase reveal addition to radical species [12] and olefins [13]. For the addition of triplet NH (produced by flash photolysis of HN_3) to C_2H_4, a thermal reaction rate constant of the order of 10^{-14} $cm^3 mol^{-1} sec^{-1}$ has been reported, whereas the abstraction of hydrogen from C_2H_4 under the same conditions is very inefficient [13]. The latter result may be rationalized for a planar configuration of the triplet $HN{-}H{-}CH{=}CH_2$ transition complex. Assuming that the $CH{=}CH_2$ group remains a spectator, denoted as Sp, the σ and π MOs of Sp remain doubly occupied

during the H abstraction by triplet NH. The formation of a planar HN–H–Sp complex involves draining the HSp bond of electrons and occupying the bonding and anti-bonding N–H–Sp MO of a' symmetry with three electrons, resulting (with a singly occupied a'' MO) in an a'' electronic state. The same energetically unfavourable electronic structure changes would occur for the HSp and NH moieties and the triplet $NH–C_2H_4$ complex during for the H-abstraction reaction.

5 Concluding remarks

We have presented high-level MCSCF calculations of the intrinsic reaction path for the reaction $^3NH + H_2 \rightarrow NH_2 + H$ and thermal rate constants computed in the harmonic approximation of the MCSCF reaction-path potential. The complete active space calculations of the lowest electronic state of $^3NH_3$ include dynamic correlation of the eight valence electrons and correctly describe the change of the electronic structure along the IRP.

The IRP describes repulsive configurations for the hydrogen abstraction and a saddle point which is located late in the reaction path. The reaction is endothermic by 11.0 kcal mol^{-1} and the IRP has a substantial barrier of 23.4 kcal mol^{-1}. The calculated change of the internal energy for this reaction and the geometries of the fragments agree very well with the available experimental data. Classical variational transition state theory calculations of the rate constants in the temperature range 400–2500 K predict this reaction to be very inefficient; being two orders of magnitude smaller than those of the $OH + H_2$ reaction.

Acknowledgments. J. I. acknowledges the financial support by the Deutsche Forschungsgemeinschaft (DFG) and the Auckland University Research Committee. J. I. and P. S. are very grateful to the Alexander von Humboldt-Foundation (Bonn).

References

1. Miller WH, Handy NC, Adams JE (1980) J Chem Phys 72:99
2. Garrett BC, Truhlar DG, Grev RS (1981) In: (ed) Truhlar DG, Potential energy-surface and dynamics calculations. Plenum, New York; (b) Isaacson AD and Truhlar DG (1982) J Chem Phys 76:1380; (c) Truhlar DG, Garrett BC (1984) Ann Phys Rev Chem 35:159
3. Fukui K, J Chem Phys (1970) 74:4161
4. (a) Page M, McIver JW (1988) J Chem Phys 88:922; (b) Ischtwan J, Collins MA (1988) J Chem Phys 89:2881
5. Natanson GA, Garrett BC, Truong TN, Joseph T, Truhlar DG (1991) J Chem Phys 94:7875
6. Bettendorf M, Peyerimhoff SD, Buenker RJ (1982) Chem Phys 66:261
7. (a) Buenker RJ, Peyerimhoff SD (1974) Theor Chim Acta 35:33; (b) Buenker RJ, Peyerimhoff SD (1975) Theor Chim Acta 39:217; (c) Buenker RJ, Peyerimhoff SD, Butscher W (1978) Mol Phys 35:771
8. (a) Wahl AC, Das G (1977) In: Schaefer III HF (ed) Methods of electronics structure theory. Plenum, New York; (b) Roos BO, Taylor PR, Siegbahn PEM (1980) Chem Phys 48:157
9. Jensen HJ Aa, Ågren H, SIRIUS: A general purpose MCSCF program, MOTECC-90. IBM Corporation, Kingston, New York
10. Helgaker T, Jensen HJ Aa, Jørgensen P, Olsen J, Taylor P (1991) ABACUS – A second order MCSCF property program, release 1 Feb 1991, Oslo, Norway
11. (a) Fueno T, Bonacic-Koutecky V, Koutecky J (1983) J Am Chem Soc 105:5547; (b) Fueno T, Bonacic-Koutecky V, Koutecky J (1984) J Am Chem Soc 106:4061
12. Hansen I, Höinghaus K, Zetsch C, Stuhl F (1976) Chem Phys Lett 42:370

13. Cornell DW, Berry RS, Lwowski W (1966) J Am Chem Soc 88:544
14. For a general description of basis sets and ab initio molecular orbital methods see for example: Hehre WJ, Radom L, Schleyer PvR, Pople JA (1986) Ab initio molecular orbital theory. Wiley, New York
15. Jensen HJ Aa, Jørgensen P, Ågren H, Olsen J (1987) J Chem Phys 88:3834
16. Dunning T Jr (1971) J Chem Phys 55:716
17. Frisch MJ, Head-Gordon M, Trucks GW, Foresman JB, Schlegel HB, Raghavachari K, Robb MA, Binkley JS, Gonzalez C, Defrees DJ, Fox DJ, Whiteside RA, Seeger R, Melius CF, Baker J, Kahn RL, Stewart JJP, Topiol S, Pople JA (1990) GAUSSIAN 90. Gaussian, Pittsburgh, PA
18. Hammond GS (1955) J Am Chem Soc 77:334
19. Chase MW Jr, Davies CA, Downey JR Jr, Frurip DJ, McDonald RA, Syverup AN (1985) JANAF thermochemical tables, 3rd ed, J Phys Chem Ref Data 14 (1), New York
20. Eckart C (1930) Phys Rev 35:1303
21. (a) Pollak E, Pechukas P (1978) J Am Chem Soc 100:2984; (b) Coulson DR (1978) J Am Chem Soc 100:2992
22. Isaacson AD (1992) J Phys Chem 96:531
23. Schatz GC, Colton MC, Grant JL (1984) J Phys Chem 88:2971